

Energy adaptive regulation of a multifunctional neuron circuit

Xi-kui Hu(胡锡奎), Juan Yang(杨娟), and Ping Zhou(周平)

Citation: Chin. Phys. B, 2026, 35 (**1**): 010503. DOI: 10.1088/1674-1056/ae1451
http://cpb.iphy.ac.cn; http://iopscience.iop.org/cpb

What follows is a list of articles you may be interested in

Synchronous dynamics of robotic arms driven by Chua circuits

Guoping Sun(孙国平), Mingxin Xu(许明鑫), Guoqiang Jin(金国强), and Xufeng Wang(王旭峰)
Chin. Phys. B, 2025, 34 (**6**): 060501. DOI: 10.1088/1674-1056/adc2e1

Bifurcation analysis and control study of improved full-speed differential model in connected vehicle environment

Wen-Huan Ai(艾文欢), Zheng-Qing Lei(雷正清), Dan-Yang Li(李丹洋), Dong-Liang Fang(方栋梁), and Da-Wei Liu(刘大为)
Chin. Phys. B, 2024, 33 (**7**): 070503. DOI: 10.1088/1674-1056/ad3b80

Bifurcation analysis of visual angle model with anticipated time and stabilizing driving behavior

Xueyi Guan(管学义), Rongjun Cheng(程荣军), and Hongxia Ge(葛红霞)
Chin. Phys. B, 2022, 31 (**7**): 070507. DOI: 10.1088/1674-1056/ac5606

Modeling and dynamics of double Hindmarsh-Rose neuron with memristor-based magnetic coupling and time delay

Guoyuan Qi(齐国元) and Zimou Wang(王子谋)
Chin. Phys. B, 2021, 30 (**12**): 120516. DOI: 10.1088/1674-1056/ac16cc

Experimental identification of a comb-shaped chaotic region in multiple parameter spaces simulated by the Hindmarsh–Rose neuron model

Jia Bing (贾冰)
Chin. Phys. B, 2014, 23 (**3**): 030505. DOI: 10.1088/1674-1056/23/3/030505

SPECIAL TOPIC — Biophysical circuits: Modeling & applications in neuroscience

Energy adaptive regulation of a multifunctional neuron circuit

Xi-Kui Hu(胡锡奎)[†], Juan Yang(杨娟), and Ping Zhou(周平)

School of Electronic Science and Engineering, Chongqing University of Posts and Telecommunications, Chongqing 400065, *China*

(Received 19 August 2025; revised manuscript received 1 October 2025; accepted manuscript online 17 October 2025)

This study constructs a dual-capacitor neuron circuit (connected via a memristor) integrated with a phototube and a thermistor to simulate the ability of biological neurons to simultaneously perceive light and thermal stimuli. The circuit model converts photothermal signals into electrical signals, and its dynamic behavior is described using dimensionless equations derived from Kirchhoff's laws. Based on Helmholtz's theorem, a pseudo-Hamiltonian energy function is introduced to characterize the system's energy metabolism. Furthermore, an adaptive control function is proposed to elucidate temperature-dependent firing mechanisms, in which temperature dynamics are regulated by pseudo-Hamiltonian energy. Numerical simulations using the fourth-order Runge–Kutta method, combined with bifurcation diagrams, Lyapunov exponent spectra, and phase portraits, reveal that parameters such as capacitance ratio, phototube voltage amplitude/frequency, temperature, and thermistor reference resistance significantly modulate neuronal firing patterns, inducing transitions between periodic and chaotic states. Periodic states typically exhibit higher average pseudo-Hamiltonian energy than chaotic states. Two-parameter analysis demonstrates that phototube voltage amplitude and temperature jointly govern firing modes, with chaotic behavior emerging within specific parameter ranges. Adaptive control studies show that gain/attenuation factors, energy thresholds, ceiling temperatures, and initial temperatures regulate the timing and magnitude of system temperature saturation. During both heating and cooling phases, temperature dynamics are tightly coupled with pseudo-Hamiltonian energy and neuronal firing activity. These findings validate the circuit's ability to simulate photothermal perception and adaptive temperature regulation, contributing to a deeper understanding of neuronal encoding mechanisms and multimodal sensory processing.

Keywords: photothermal sensing neuron, pseudo-Hamiltonian energy, chaotic firing, adaptive temperature control, bifurcation analysis

PACS: 05.45.–a, 05.45.Pq, 05.45.Gg

DOI: 10.1088/1674-1056/ae1451 **CSTR:** 32038.14.CPB.ae1451

1. Introduction

The brain is a complex neural network, with neurons serving as the fundamental units for information processing.[1] Biological neurons possess a physiological foundation for multimodal perception. Neurons, as the core functional units of the nervous system, maintain multiple functions because their structural specialization and the demands of neural system operation force them to integrate diverse roles. The biological nervous system can efficiently integrate various sensory information, such as light, heat, and touch, to achieve complex environmental perception and decision-making.[2] With the rapid development of neuroscience and artificial intelligence, simulating the multimodal perception ability of biological neurons has become a research highlight.[3] Among them, neuron models that simultaneously perceive photothermal effects have received widespread attention due to their extensive potential applications in biomimetic perception, intelligent sensors, and neuromorphic computing.[4] Photothermal sensing refers to the ability of neurons to respond simultaneously to both light and heat signals and convert these two physical stimuli into electrical signals for processing. This ability is widely present in nature. For instance, the infrared sensing system of snakes can simultaneously detect changes in light and environmental temperature, enabling precise positioning and predation in complex environments.[5] Certain proteins in organisms can control cells to simultaneously exhibit photothermal effects. For instance, opsin 5 in neurons of the mouse preoptic area is sensitive to visible violet light, which regulates thermogenesis in brown adipose tissue.[6] Inspired by this, researchers have begun to explore how to simulate this multimodal perception ability through artificial neural models and apply it to fields such as robot perception,[7] environmental monitoring,[8] and efficient computing.[9] For example, photothermal modulation is a remote and non-genetic approach with high spatiotemporal resolution for controlling neural activity, which provides crucial insights for guiding the establishment of light conditions and protocols in the clinical translation of photothermal modulation.[10]

By studying neuronal circuits, we can comprehensively understand how the brain accomplishes intricate functions such as perception, cognition, and memory. With the advancement of electronic technology, researchers have begun

[†]Corresponding author. E-mail: huxk@cqupt.edu.cn

© 2026 Chinese Physical Society and IOP Publishing Ltd. All rights, including for text and data mining, AI training, and similar technologies, are reserved.

to utilize electronic components to construct simple neural circuit models, aiming to simulate the fundamental functions of neurons.[11] Traditional neural models mainly focus on the transmission of electrical signals while ignoring the multimodal perception ability of neurons toward external environmental factors such as light, heat, and pressure. In recent years, with the development of sensor technology and neuromorphic computing, researchers have started to embed various sensors in neural circuits to simulate the multimodal sensing functions of biological neurons.[12–16] Embedding phototubes into neural circuits allows neurons to respond to external light signals, which has important applications in the study of light-controlled neural circuits and optogenetics.[13] Embedding thermistors into neural circuits can simulate the response of biological neurons to temperature and facilitate the study of temperature effects on neuronal firing patterns.[14] Embedding gas sensors into neural circuits can simulate the perception ability of biological neurons toward odor signals, providing a new tool for studying olfactory perception.[15] Embedding piezoelectric ceramics into neural circuits enables the capture of external acoustic signals and further establishes a binaural auditory system via parallel circuit coupling composed of Josephson junctions and linear resistors.[16] These types of neurons with biophysical functions can not only perceive and process various physical signals but also provide new possibilities for developing more intelligent perception and computing systems. However, to achieve multimodal perception capabilities closer to those of biological neurons, it is necessary to develop a neuron circuit that can simultaneously process multiple perception signals, such as one that can perceive both light and heat. The construction of a multifunctional neuron model aims to simulate the integrated perception mechanisms of biological neurons, thereby enhancing the environmental adaptability of artificial neural networks.

On the other hand, the cell membrane plays a crucial role in the process of information transmission. Traditional neuronal models typically simplify the cell membrane into a single capacitor. However, the cell membrane of biological neurons is an elastic structure composed of lipid bilayers.[17] There are differences in electrical properties between the inner and outer layers of the cell membrane. Therefore, traditional single-capacitance models cannot fully reflect the double-layer structure and complex physical properties of the cell membrane. In recent years, researchers have proposed dual-capacitor neuron membrane models, which simulate the inner and outer bilayer structure of the cell membrane by introducing two capacitors. The two-capacitor structure can more realistically represent the double-layer structure of cell membranes and more accurately describe the electrophysiological behavior of neurons. This model not only better explains the firing patterns of neurons but also provides a new theoretical framework for studying the energy regulation and multimodal perception of neurons. Numerous studies have demonstrated that both linear and nonlinear electronic components can be utilized to connect two capacitors to investigate neural activity induced by cell membrane deformation and modal transitions, such as Josephson junctions, linear resistors, nonlinear resistors, and memristors.[18–21] Memristors, as a novel type of electronic component, exhibit variable resistance characteristics that resemble the synaptic behavior of biological neurons.[22] Researchers have begun to apply memristors in the construction of neuronal circuits, enabling the storage and processing of neural signals.[23–25] By incorporating one or two memristors into the branches of a nonlinear circuit, it is possible to modulate the channel current between capacitive and inductive elements, thereby altering the energy distribution among these electronic components.[26–28] Consequently, the integration of memristors within functional neuronal circuits can effectively regulate the energy ratio between the inner and outer membranes, thereby enhancing the model's ability to describe the dynamics of membrane potential and energy metabolism.

In this paper, a phototube and a thermistor are integrated into a dual-capacitor neuron circuit connected by a memristor to construct a neuron circuit that can simultaneously sense external light stimulation and system temperature changes. Phototubes can capture external light and simulate light signals to stimulate neural pathways. The resistance value of a thermistor changes with temperature, which can be used to detect temperature variations. Therefore, by embedding the phototube and thermistor in the corresponding branches, the neuron circuit can simultaneously sense photothermal signals and convert them into electrical signals for processing. The circuit model can simulate the ability of biological neurons to perceive light and heat simultaneously, improve perception accuracy and the intelligence level of the system, and has broad application prospects in fields such as bionic sensors, medical equipment, environmental monitoring, smart homes, and artificial intelligence.

In addition, the temperature and energy metabolism of neurons are closely related. Temperature changes affect neuronal function, thereby altering energy demand and production. In actual neuronal systems, neurons consume energy to generate and transmit action potentials for information coding, transmission, and processing.[26–28] The utilization and consumption of energy directly affect the information processing capability of neurons. Therefore, changes in system energy influence intrinsic neuronal parameters (such as temperature), thereby establishing appropriate neuron firing patterns. Specifically, the activity and channel currents of sodium and potassium ion channels vary with temperature, resulting in different firing patterns and changes in neuronal excitability un-

der different thermal conditions. Consequently, adaptive regulation of neuron temperature based on energy variation in a photothermal sensing neuron circuit is worthy of further study.

2. Model and scheme

The schematic diagram of a dual-capacitor neuron circuit with photothermal sensing is shown in Fig. 1. The cellular membrane exhibits a bilayer structure, and its physical field characteristics can be described in terms of two capacitors, marked as C_1 and C_2, respectively. Memristors are employed in the circuit to connect the two capacitors. The phototube functions as a voltage source. The thermistor is used to replace the linear resistor to sense thermal effects. An induction coil generates a time-varying current within the branch, and a nonlinear resistor is utilized to capture the nonlinear relationship between voltage and current. The photodiode is activated when exposed to external light, generating a sustained photovoltage that stimulates the neural circuit. Simultaneously, changes in external temperature modulate the thermistor's resistance. Due to the characteristics of the thermistor, an increase in temperature enhances the activity of internal charge carriers, leading to a reduction in resistance. Conversely, a decrease in temperature restricts carrier activity, thereby increasing resistance. This dynamic variation in resistance further influences the current within the circuit, triggering a time-varying channel current, which causes the circuit's current state to continuously change with temperature and provides a crucial response mechanism for the dynamic regulation of the entire circuit system.

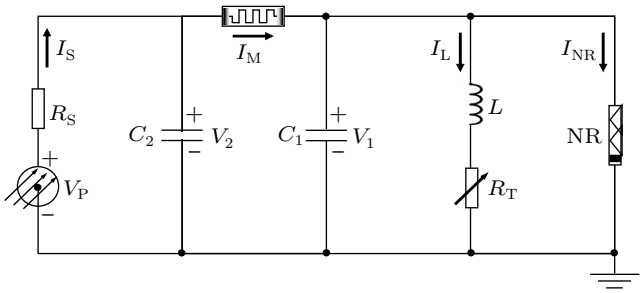


Fig. 1. Schematic diagram of the dual-capacitor neuron circuit with photothermal sensing. V_P denotes a phototube, R_S represents a linear resistor, C_1 and C_2 are capacitors, M signifies a memristor, L is an inductor, R_T indicates a thermistor, and NR is a nonlinear resistor.

According to Kirchhoff's laws, the relationships between the physical variables of the neuron circuit shown in Fig. 1 are presented as

$$\begin{cases} C_1 \dfrac{\mathrm{d}V_1}{\mathrm{d}t} = I_M - I_L - I_{NR}, \\ C_2 \dfrac{\mathrm{d}V_2}{\mathrm{d}t} = I_S - I_M = \dfrac{V_P - V_2}{R_S} - I_M, \\ L \dfrac{\mathrm{d}I_L}{\mathrm{d}t} = V_1 - R_T I_L. \end{cases} \tag{1}$$

The current of the magnetically controlled memristor connecting the two capacitors is denoted by I_M and is defined as follows:[29]

$$\begin{cases} I_M = M_\Phi V_M = (A + 3B\Phi^2)(V_2 - V_1), \\ \dfrac{\mathrm{d}\Phi}{\mathrm{d}t} = V_M = (V_2 - V_1). \end{cases} \tag{2}$$

The variable Φ represents the magnetic flux, and $M_\Phi = (A + 3B\Phi^2)$ denotes the conductivity of the memristor. The physical parameters A and B are related to the material properties of the memristor.

The current in the nonlinear resistor is denoted by I_{NR} and has the following functional relationship:[29]

$$I_{NR} = -\frac{1}{\rho}\left(V_1 - \frac{1}{3}\frac{V_1^3}{V_0^2}\right), \tag{3}$$

where ρ is the normalized resistance parameter, and V_0 represents the cut-off voltage. When the voltage V_1 reaches the cut-off voltage, the current I_{NR} is cut off or significantly reduced.

The phototube receives external light signals and generates a time-varying current, which can be regarded as a time-varying voltage or current source in the neuron circuit.[30] As shown in Fig. 1, the activated phototube is modeled as a time-varying voltage source. The photocurrent emitted by the phototube is controlled by external illumination. Accordingly, the output voltage V_P of the phototube in this functional neuron circuit can be adjusted by external light and is defined as follows:[30]

$$V_P = U_0 \cos \omega' t. \tag{4}$$

The amplitude U_0 and angular frequency ω' can be adjusted by the external illumination intensity and the coating on the cathode material of the phototube. The cosine function is used to simulate the output voltage of a photoelectric cell when it is excited by periodic light signals (e.g., from a flickering light source), and its amplitude is adjustable.

An increase in temperature usually leads to an increase in the maximum conductivity of neuronal ion channels and faster activation and deactivation rates.[31] Therefore, a thermistor with a negative temperature coefficient is selected in the neuron circuit shown in Fig. 1, and its functional relationship is defined as[32]

$$R_T = R_0 \exp\left(T_c\left(\frac{1}{T'} - \frac{1}{T_0'}\right)\right), \tag{5}$$

where R_T is the resistance of the thermistor at the operating temperature T', R_0 is the resistance of the thermistor at the reference temperature T_0', and T_C is the temperature constant related to the physical properties of the thermistor material. When the reference temperature of the thermistor T_0' is much

higher than the operating temperature T', Eq. (5) can be simplified as

$$R_{\mathrm{T}} = R_0 \exp\left(\frac{T_{\mathrm{c}}}{T'}\right). \tag{6}$$

Through standard scaling transformations, the physical variables and parameters in the previous equations are rendered dimensionless. These physical variables and parameters are substituted as

$$\begin{cases} x = \dfrac{V_1}{V_0}, y = \dfrac{V_2}{V_0}, z = \dfrac{\rho I_{\mathrm{L}}}{V_0}, \phi = \dfrac{\Phi}{\rho C_1 V_0}, \\ \tau = \dfrac{t}{\rho C_1}, \omega = \rho C_1 \omega', a = \rho A, b = \rho^3 C_1^2 V_0^2 B, \\ c = \dfrac{C_1}{C_2}, \eta = \dfrac{\rho}{R_S}, l = \dfrac{\rho^2 C_1}{L}, \\ u_{\mathrm{P}} = \dfrac{V_{\mathrm{P}}}{V_0}, u_0 = \dfrac{U_0}{V_0}, r = \dfrac{R_{\mathrm{T}}}{\rho}, r_0 = \dfrac{R_0}{\rho}, T = \dfrac{T'}{T_{\mathrm{c}}}. \end{cases} \tag{7}$$

The dynamic behavior of the physical variables of the neuron circuit shown in Fig. 1 can be studied using the following dimensionless system:

$$\begin{cases} \dfrac{\mathrm{d}x}{\mathrm{d}\tau} = \left(a + 3b\phi^2\right)(y - x) - z + x - \dfrac{1}{3}x^3, \\ \dfrac{\mathrm{d}y}{\mathrm{d}\tau} = c\left[\eta\left(u_{\mathrm{P}} - y\right) - \left(a + 3b\phi^2\right)(y - x)\right], \\ \dfrac{\mathrm{d}z}{\mathrm{d}\tau} = l\left(x - rz\right), \\ \dfrac{\mathrm{d}\phi}{\mathrm{d}\tau} = y - x, \end{cases} \tag{8}$$

where u_{P} is the dimensionless output voltage of the phototube, and r is the dimensionless resistance of the thermistor. Their functional relationships are given by

$$\begin{cases} u_{\mathrm{P}} = u_0 \sin \omega\tau, \\ r = r_0 \exp\left(\frac{1}{T}\right). \end{cases} \tag{9}$$

The nonlinear dynamics of Eq. (8) can be analyzed using bifurcation diagrams and the Lyapunov exponent (LE) spectrum. In general, Lyapunov exponents can be calculated using the QR decomposition method,[33] and the Jacobian matrix of the system is given by

$$\boldsymbol{J} = \begin{pmatrix} -\left(a + 3b\phi^2\right) + 1 - x^2 & a + 3b\phi^2 & -1 & 6b\phi\,(y - x) \\ c\left(a + 3b\phi^2\right) & -c\eta - \left(a + 3b\phi^2\right) & 0 & -6bc\phi\,(y - x) \\ l & 0 & -lr & 0 \\ -1 & 1 & 0 & 0 \end{pmatrix}. \tag{10}$$

The physical properties of neuron circuits can be effectively characterized using the pseudo-Hamiltonian energy function $H(x, y, z, \phi)$. The total energy W_{E} of the physical field of the neuron circuit is associated with the capacitor, inductor, and memristor elements. Accordingly, the pseudo-Hamiltonian energy of the system is expressed as[34]

$$\begin{cases} W_{\mathrm{E}} = \frac{1}{2}C_1 V_1^2 + \frac{1}{2}C_2 V_2^2 + \frac{1}{2}L I_{\mathrm{L}}^2 + \frac{1}{2}L_{\mathrm{M}} I_{\mathrm{M}}^2, \\ H = \frac{W_{\mathrm{E}}}{C_1 V_0^2} = \frac{1}{2}x^2 + \frac{1}{2c}y^2 + \frac{1}{2l}z^2 + \left(a\phi + b\phi^3\right)(y - x). \end{cases} \tag{11}$$

According to Helmholtz's theorem, the physical field energy of this neuron circuit can be expressed in the vector form shown in Eq. (11). Solving this equation yields the pseudo-Hamiltonian energy function of the system[35]

$$\begin{aligned} \begin{pmatrix} \dot{x} \\ \dot{y} \\ \dot{z} \\ \dot{\phi} \end{pmatrix} &= \begin{pmatrix} \left(a + 3b\phi^2\right)(y - x) - z + x - \frac{1}{3}x^3 \\ c\left[\eta\left(u_{\mathrm{P}} - y\right) - \left(a + 3b\phi^2\right)(y - x)\right] \\ l\left(x - rz\right) \\ y - x \end{pmatrix} \\ &= f_{\mathrm{c}} + f_{\mathrm{d}} \\ &= \begin{pmatrix} \left(a + 3b\phi^2\right)(y - x) - z \\ -c\left(a + 3b\phi^2\right)(y - x) \\ l\left(x - a\phi - b\phi^3\right) \\ y - x + (1 + c)\left(a\phi + b\phi^3\right) \end{pmatrix} \\ &\quad + \begin{pmatrix} x - \frac{1}{3}x^3 \\ c\eta\left(u_{\mathrm{P}} - y\right) \\ l\left(a\phi + b\phi^3 - rz\right) \\ -(1 + c)\left(a\phi + b\phi^3\right) \end{pmatrix} \\ &= \left[\begin{pmatrix} 0 & 0 & -l & 1 \\ 0 & 0 & 0 & -c \\ l & 0 & 0 & 0 \\ -1 & c & 0 & 0 \end{pmatrix} + \begin{pmatrix} A_{11} & 0 & 0 & 0 \\ 0 & A_{22} & 0 & 0 \\ 0 & 0 & A_{33} & 0 \\ 0 & 0 & 0 & A_{44} \end{pmatrix}\right] \\ &\quad \cdot \begin{pmatrix} H_x \\ H_y \\ H_z \\ H_\phi \end{pmatrix}, \end{aligned} \tag{12}$$

where the parameters in the symmetric matrix are defined as

$$\begin{cases} A_{11} = \dfrac{x - \frac{1}{3}x^3}{x - (a\phi + b\phi^3)}, \\ A_{22} = \dfrac{c^2\eta\,(u_{\mathrm{P}} - y)}{y + c(a\phi + b\phi^3)}, \\ A_{33} = \dfrac{l^2(a\phi + b\phi^3 - rz)}{z}, \\ A_{44} = \dfrac{-(1 + c)(a\phi + b\phi^3)}{(a + 3b\phi^2)(y - x)}. \end{cases} \tag{13}$$

Per Helmholtz's theorem, ∇H is the gradient vector of the

pseudo-Hamiltonian energy function $H(x,y,z,\phi)$, defined as

$$\nabla H = \begin{pmatrix} H_x \\ H_y \\ H_z \\ H_\phi \end{pmatrix} = \begin{pmatrix} \dfrac{\partial H}{\partial x} \\ \dfrac{\partial H}{\partial y} \\ \dfrac{\partial H}{\partial z} \\ \dfrac{\partial H}{\partial \phi} \end{pmatrix} = \begin{pmatrix} x-(a\phi+b\phi^3) \\ \dfrac{y}{c}-(a\phi+b\phi^3) \\ \dfrac{z}{l} \\ (a+3b\phi^2)(y-x) \end{pmatrix}. \quad (14)$$

Furthermore, the pseudo-Hamiltonian energy function satisfies the following conditions

$$\begin{aligned} \nabla H^{\mathrm{T}} f_{\mathrm{c}} =& \left[\left(a+3b\phi^2\right)(y-x)-z\right]\frac{\partial H}{\partial x} \\ & -c\left(a+3b\phi^2\right)(y-x)\frac{\partial H}{\partial y} \\ & +l\left(x-a\phi-b\phi^3\right)\frac{\partial H}{\partial z} \\ & +\left[y-x+(1+c)\left(a\phi+b\phi^3\right)\right]\frac{\partial H}{\partial \phi} \quad (15) \\ =& \ 0, \quad (16) \\ \nabla H^{\mathrm{T}} f_{\mathrm{d}} =& \left(x-\frac{1}{3}x^3\right)\frac{\partial H}{\partial x}+c\eta\left(u_{\mathrm{P}}-y\right)\frac{\partial H}{\partial y} \\ & +l\left(a\phi+b\phi^3-rz\right)\frac{\partial H}{\partial z} \\ & -(1+c)\left(a\phi+b\phi^3\right)\frac{\partial H}{\partial \phi}=\frac{\mathrm{d}H}{\mathrm{d}\tau}. \quad (17) \end{aligned}$$

It is evident that the pseudo-Hamiltonian energy function derived from Eq. (14) is equivalent to that obtained from Eq. (11). Given the energy characteristics of neurons, mode selection within the system depends on energy levels; thus, fluctuations in energy values can trigger mode transitions.

Organisms maintain body temperature stability through the dynamic balance of energy metabolism, a core mechanism by which life adapts to the environment.[36,37] There is a bidirectional feedback mechanism between energy metabolism and temperature regulation. On one hand, organisms supply energy for body movements via cellular energy metabolism while generating heat to regulate body temperature. On the other hand, temperature changes affect the rate of energy metabolism by influencing bodily activity. Additionally, the body can regulate temperature through peripheral vasodilation, sweat evaporation, and accelerated breathing. With continuous energy regulation and injection, heat accumulates over time, leading to a gradual rise in temperature.

Consistent with the fundamental principles of thermodynamics, temperature is a physical quantity that characterizes the intensity of particle thermal motion. Thus, when the pseudo-Hamiltonian energy of the nervous system increases — resulting in elevated metabolic heat production — the temperature of the nervous system changes correspondingly. Some relevant parameters can be approximately expressed as an adaptive control function[38]

$$\frac{\mathrm{d}T}{\mathrm{d}\tau} = \sigma_1 T\cdot\Theta(H-H_0)-\sigma_2\cdot\Theta(T-T_{\mathrm{m}}), \quad (18)$$

where σ_1 is the gain factor governing the rate of temperature rise, and σ_2 is the attenuation factor controlling the cooling rate. The gain factor σ_1 is analogous to the metabolic heat production rate in biological organisms (e.g., regulated by thyroid hormones), while the attenuation factor σ_2 corresponds to heat dissipation mechanisms (such as sweat gland evaporation and vasodilation). $\Theta(H-H_0)$ and $\Theta(T-T_{\mathrm{m}})$ are step functions whose values satisfy the expression below:[38]

$$\Theta(P) = \begin{cases} 1, & P \geq 0, \\ 0, & P < 0, \end{cases} \quad (19)$$

The step function, as a simplified model, can effectively reveal the energy–temperature coupling mechanism. Furthermore, smoothing functions — such as the Sigmoid function — enable a more accurate approximation of the continuity inherent in biological thermoregulation processes. However, incorporating these functions will significantly increase system complexity, and this aspect will be explored in depth in future research.

In other words, the system has an energy threshold H_0 which is equivalent to the basal metabolic rate. When the system's pseudo-Hamiltonian energy is below this threshold, the heat generated by energy metabolism equals the heat dissipated by the system; the system is in thermal equilibrium, and its temperature remains constant. When the pseudo-Hamiltonian energy exceeds this threshold, the heat generated by energy metabolism exceeds the dissipated heat, causing the total heat of the system to increase and the temperature to rise from the initial temperature T_0 over time.

Furthermore, most organisms — particularly homeothermic animals — have an upper temperature limit T_{m}, which represents the body temperature set point. Once the system temperature reaches this limit, it no longer rises. Thus, the gain factor σ_1 and attenuation factor σ_2 in Eq. (18) should satisfy $\sigma_2 > \sigma_1 T_{\mathrm{m}}$. Introducing an adaptive control function in which temperature varies with pseudo-Hamiltonian energy can enhance the dynamic responsiveness of neurons to energy changes, thereby clarifying how neurons adjust their firing behavior over time to cope with the impact of temperature changes on systemic energy metabolism.

3. Numerical results and discussion

This section examines the diverse firing patterns of the neuron model described in Eq. (8), which are obtained by

modulating external stimuli or system parameters. Numerical solutions of the model are computed using the fourth-order Runge–Kutta method. A straightforward periodic excitation of the form $u_{\rm P} = u_0 \cos(\omega\tau)$ is employed to stimulate the neuron circuit system. The benchmark parameters are $\omega = 0.4\pi$, $a = 0.05$, $b = 0.05$, $c = 1.5$, $\eta = 0.2$, $l = 0.2$, $u_0 = 5$, $r_0 = 0.8$, and $T = 5$, with initial values $(0.2, 0.1, 0.02, 0.01)$. For the simulations conducted in this study, a time step of $\Delta\tau = 0.01$ is adopted, and the final simulation duration is set to $T_{\rm f} = 1000$. To ensure clarity in result presentation, only the data corresponding to the first 400 time units are displayed in the time evolution figures.

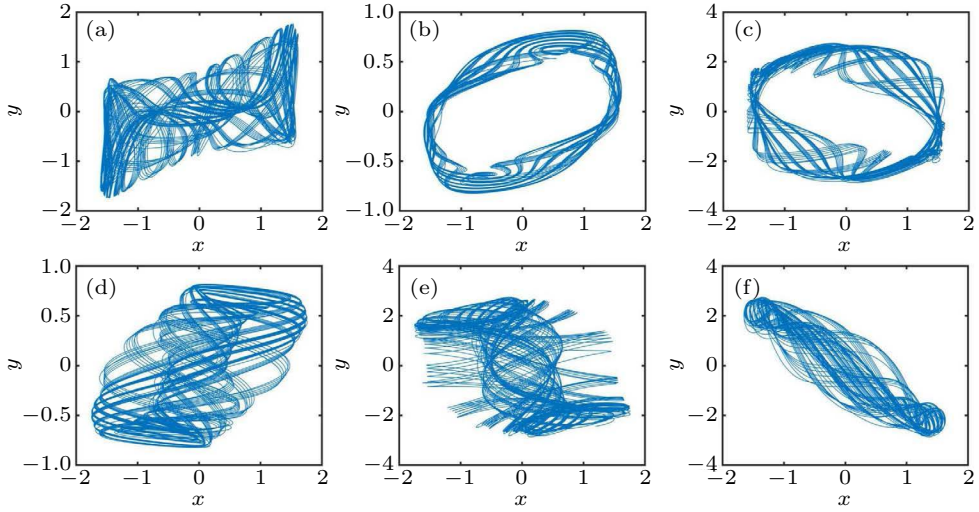


Fig. 2. Phase portraits of the neuron circuit system in different phase-space planes. Parameters used are $\omega = 0.4\pi$, $a = 0.05$, $b = 0.05$, $c = 1.5$, $\eta = 0.2$, $l = 0.2$, $u_0 = 5$, $r_0 = 0.8$, and $T = 5$.

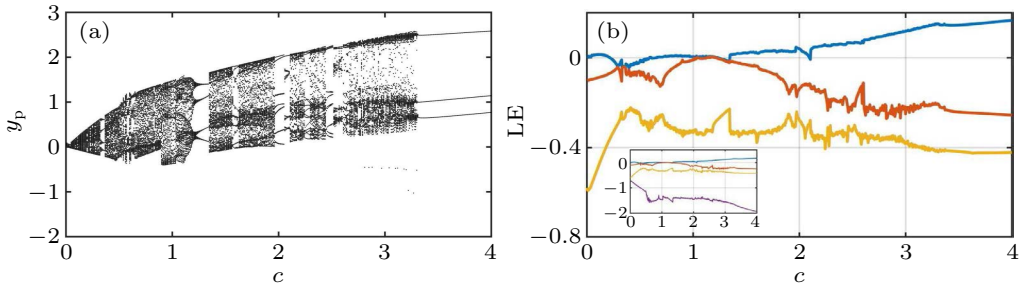


Fig. 3. Dynamics of the neuron circuit under varying capacitance ratios of the two capacitors. (a) Bifurcation diagram; (b) three largest Lyapunov exponents, with the full set shown in the inset.

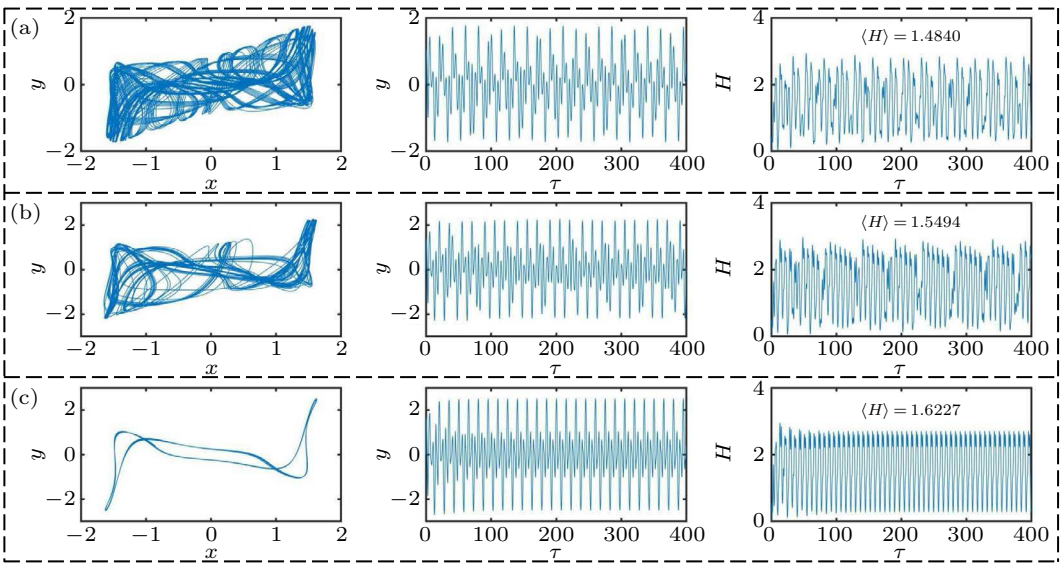


Fig. 4. Evolution of the neuron circuit in the x–y phase plane, along with the variable y and pseudo-Hamiltonian energy H, for different capacitance ratios: (a) $c = 1.5$; (b) $c = 2.5$; (c) $c = 3.5$.

Phase diagrams depict the temporal dynamics of a system by plotting trajectories in a phase space defined by its state variables. The curves in Fig. 2 represent system trajectories projected onto different pairs of state variables. Each subplot displays trajectories in a plane spanned by two state variables, thereby reflecting the system's dynamic behavior in the corresponding dimensions. Among them, the trajectories in the x–y plane phase diagram are characterized by pronounced curve entanglement, which effectively reveals intricate dynamical behaviors (e.g., chaos). Therefore, the x–y plane phase diagram is adopted for subsequent analysis.

In bilayer membrane neurons, variations in the capacitance ratio c can induce memory neurons to exhibit periodic and chaotic firing patterns (Fig. 3). For clarity, the Lyapunov exponent spectra present only the temporal evolution of the three largest exponents, while the complete set of exponents is shown in the inset.

Careful adjustment of the capacitance ratio c can further trigger significant pattern transitions (Fig. 4). When $c = 1.5$ and $c = 2.5$, the attractor trajectories exhibit complex, aperiodic behavior indicative of strong chaotic dynamics, with high-frequency membrane potential oscillations that lack a fixed period, consistent with chaotic attractors. In contrast, at $c = 3.5$, the attractor collapses onto a regular closed curve, corresponding to a periodic state. In this regime, the capacitance ratio stabilizes the effective time constant associated with the membrane capacitance, resulting in periodic neuronal firing, which may support specific rhythmic neural activities.

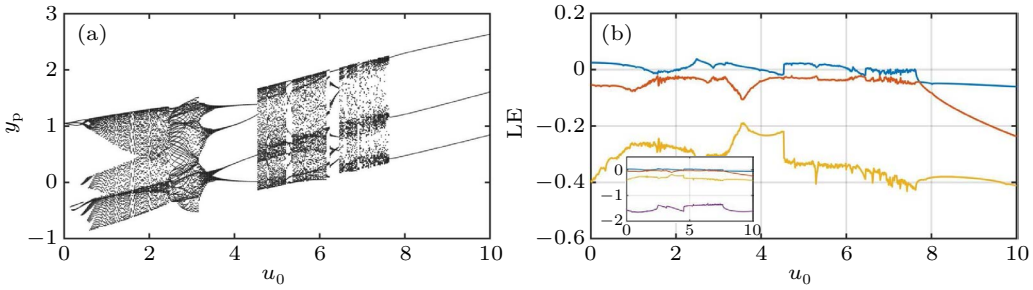


Fig. 5. Dynamics of the neuron circuit under different phototube output voltage amplitudes. (a) Bifurcation diagram; (b) three largest Lyapunov exponent spectra, with the complete set shown in the inset.

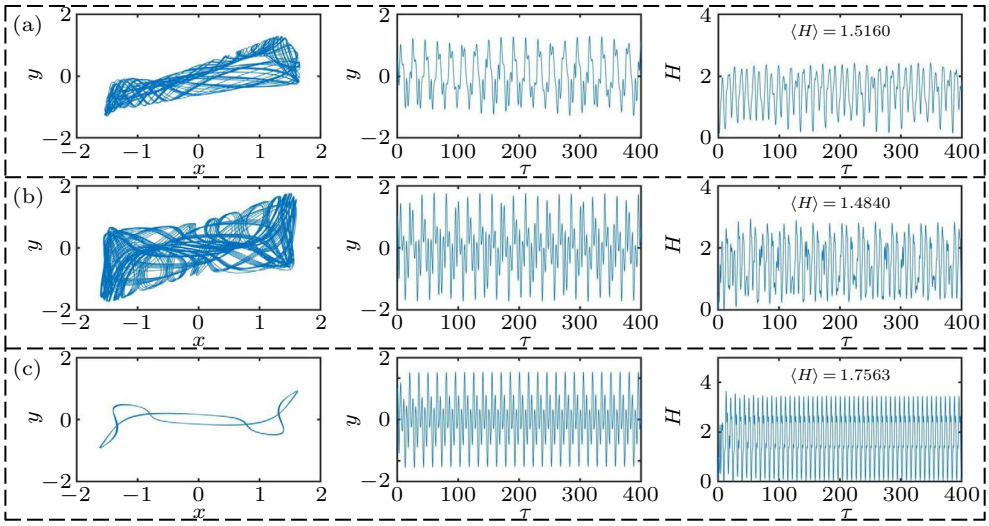


Fig. 6. Evolution of x–y phase portraits, variable y, and pseudo-Hamiltonian energy H under different phototube output voltage amplitudes: (a) $u_0 = 2$; (b) $u_0 = 5$; (c) $u_0 = 8$.

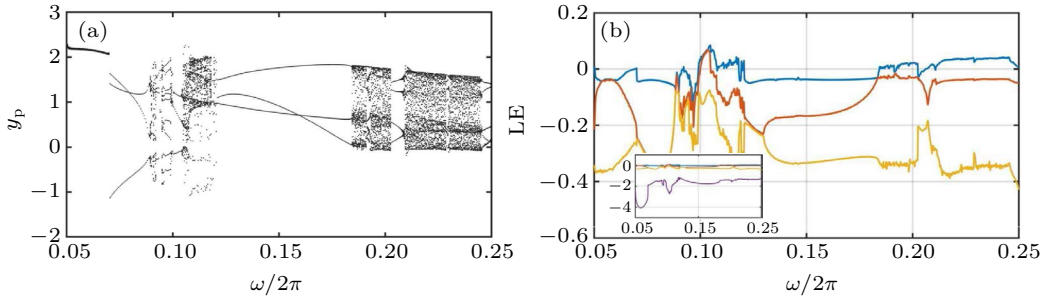


Fig. 7. Dynamics analysis under different phototube output voltage frequencies. (a) Bifurcation diagram; (b) three Lyapunov exponent spectra, with the complete set provided in the inset.

Biological neurons respond nonlinearly to variations in external stimulus intensity. As shown in Fig. 5, changing the amplitude of the external stimulus under a fixed temperature induces pronounced mode transitions: at lower amplitudes, the system exhibits chaotic firing, whereas increasing amplitude drives dynamics toward multi-periodic states, revealing the intricate dependence of neuronal firing on stimulus strength. Figure 6 further shows that appropriate tuning of voltage amplitude can shift firing patterns from chaos to periodicity, with the periodic regime exhibiting higher average pseudo-Hamiltonian energy than the chaotic regime, indicating enhanced energy accumulation during ordered firing sequences.

Modulation of the external stimulus frequency likewise governs neuronal firing modes (Fig. 7). Within certain frequency intervals, the system displays various firing patterns depending on the selected frequency. Neurons adjust responses to oscillatory signals from the phototube through voltage frequency changes, producing either chaotic or multi-periodic firing behaviors (Fig. 8). Notably, regardless of whether transitions are induced by amplitude or frequency variations, periodic firing states generally maintain higher average pseudo-Hamiltonian energy than chaotic states, suggesting rhythmic firing allows more efficient energy utilization.

System temperature variations influence peak distributions, primarily due to temperature-dependent modulation of ion channel kinetics, membrane capacitance, and other critical biophysical properties. The thermistor's resistance decreases with increasing temperature, directly affecting overall excitability and firing responsiveness. Figure 9, including the bifurcation diagram and Lyapunov exponent spectra, reveals distinct firing patterns across temperatures. By carefully adjusting temperature, the system can be driven into periodic or chaotic firing states, depending on intrinsic properties and stimulus conditions, demonstrating the temperature-sensitive nature of neuronal dynamics (Fig. 10).

The reference resistance of the thermistor also plays a critical role in shaping neuronal firing patterns. Figure 11 illustrates the relationship between neuronal firing modes and the thermistor's reference resistance. Within a certain range, an excessively high thermistor reference resistance (Fig. 12(c)) reduces conductance, substantially lowering neuronal excitability and inducing a quasi-resting state (near-resting with minimal spiking). Conversely, within an appropriate range of thermistor reference resistance, the system exhibits diverse firing patterns, revealing complex nonlinear dynamics depending sensitively on both temperature and voltage. These findings highlight the delicate balance between thermal and electrical parameters in regulating neuronal activity (Fig. 12).

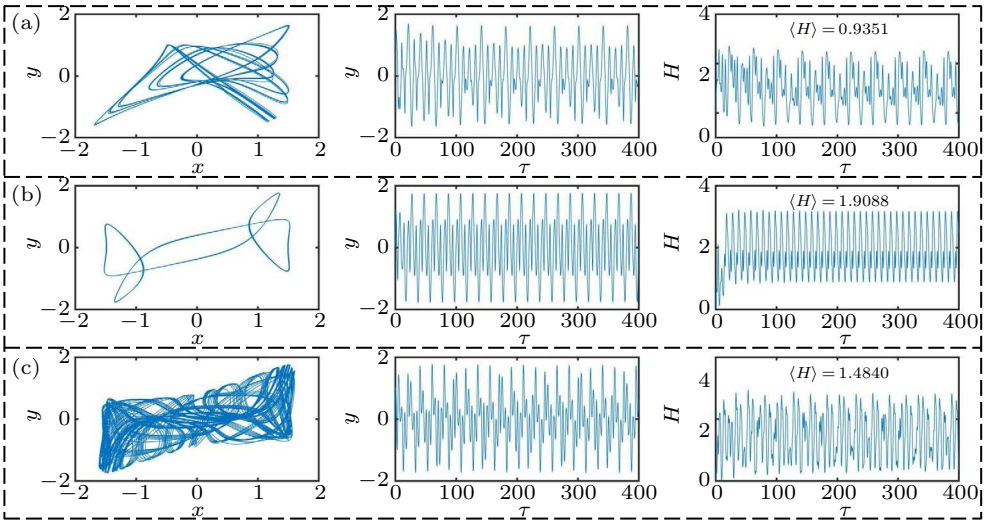


Fig. 8. Evolution of x–y plane phase portraits, variable y, and pseudo-Hamiltonian energy H at different phototube output voltage frequencies: (a) $\omega = 0.2\pi$; (b) $\omega = 0.3\pi$; (c) $\omega = 0.4\pi$.

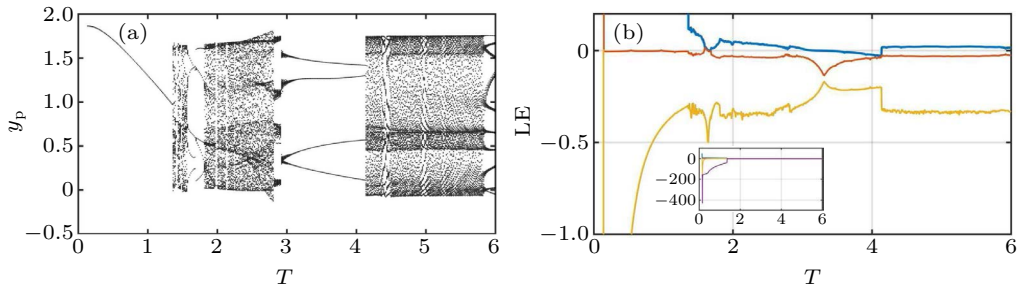


Fig. 9. Dynamics analysis at different thermistor temperatures. (a) Bifurcation diagram; (b) three Lyapunov exponent spectra, with the complete set provided in the inset.

Furthermore, a stability analysis of the system's dynamic behaviors, including phase portraits, bifurcation diagrams, and Lyapunov exponents, was performed under varying initial conditions. The results indicate that these dynamic behaviors are largely insensitive to changes in initial values, thereby enhancing the robustness of our findings.

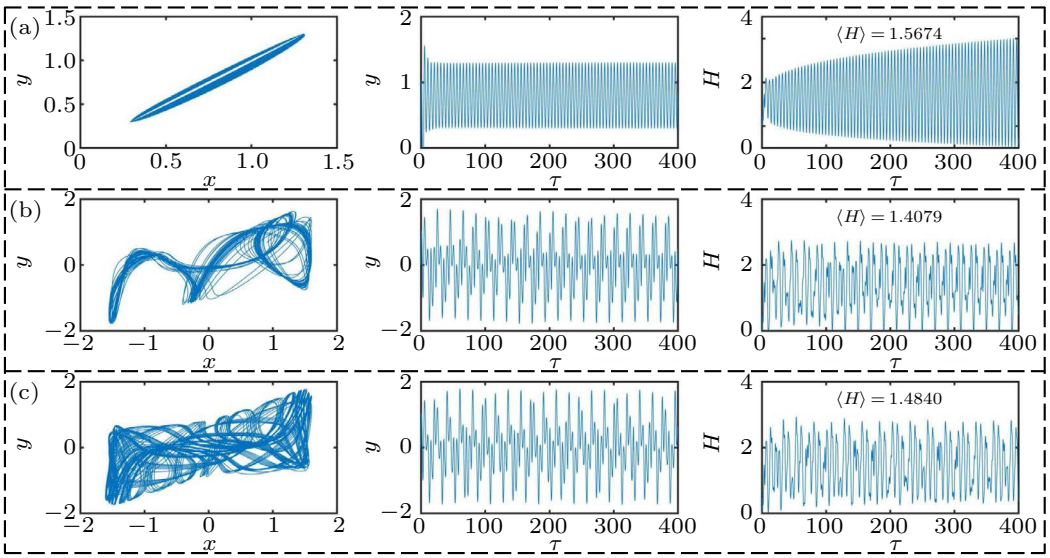


Fig. 10. Evolution of x–y plane phase portraits, variable y, and pseudo-Hamiltonian energy H at different thermistor temperatures: (a) $T = 1$; (b) $T = 3$; (c) $T = 5$.

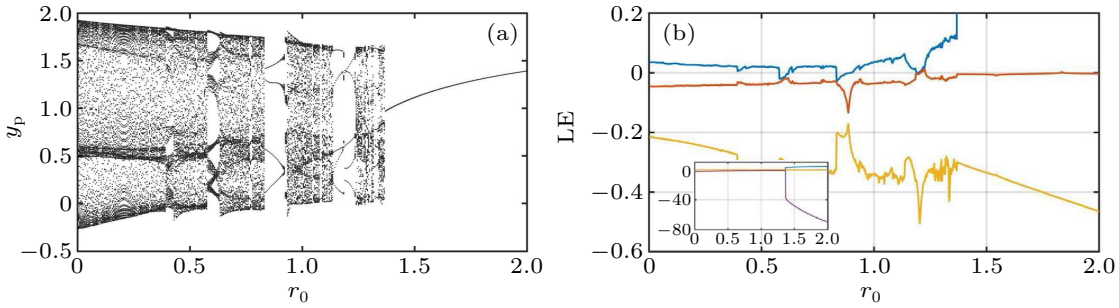


Fig. 11. Dynamics analysis for different thermistor reference resistances. (a) Bifurcation diagram; (b) three Lyapunov exponent spectra, with the complete set provided in the subfigure.

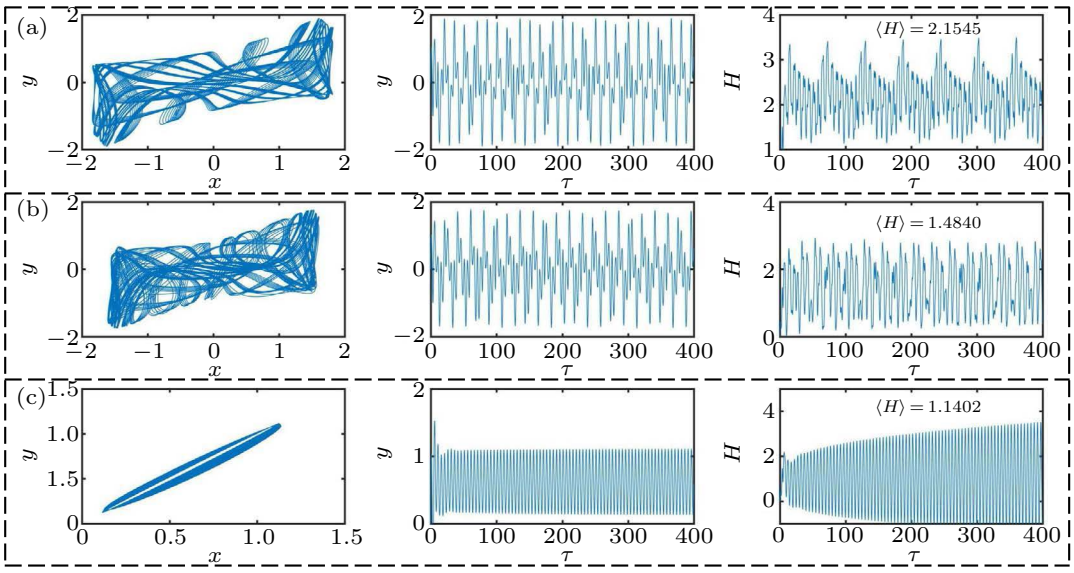


Fig. 12. Evolution of x–y plane phase portraits, variable y, and pseudo-Hamiltonian energy H for different thermistor reference resistances: (a) $r_0 = 0.1$; (b) $r_0 = 0.8$; (c) $r_0 = 1.5$.

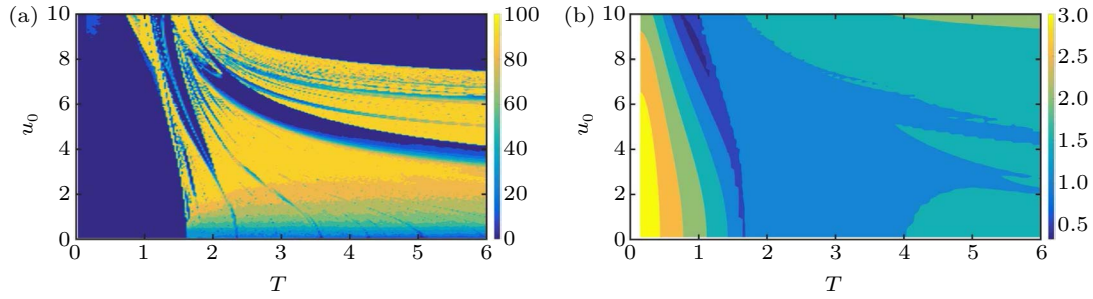


Fig. 13. Two-parameter dynamics analysis for varying phototube voltage amplitudes (u_0) and temperatures (T). Color mapping represents either the number of distinct peak magnitudes or the average pseudo-Hamiltonian energy. (a) Two-parameter bifurcation diagram; (b) average pseudo-Hamiltonian energy.

For this photothermal-sensing neuron circuit, the simultaneous perception of external light and thermal stimuli is particularly noteworthy. In Fig. 13(a), color variations represent counts of distinct peak magnitudes, with yellow regions indicating chaotic behavior (high peak counts). The two-parameter bifurcation diagram captures not only single-parameter bifurcation evolution but also the complex dynamics arising from simultaneous variation of two parameters. It demonstrates that firing states are jointly influenced by phototube voltage amplitude and temperature: vertically, temperature modulates the range of phototube voltage amplitudes associated with chaotic firing. At lower temperatures, ion channel activity is reduced, resulting in a stable quasi-quiescent state regardless of stimulus intensity. As temperature rises, the dynamic behavior transitions, including chaos, depending on the chosen stimulus intensity. Horizontally, phototube voltage amplitude modulates the temperature range for chaotic firing. Consequently, chaotic firing in functional neurons requires suitable combinations of both bifurcation parameters. Several boundary regions, representing the system's bifurcation points, are discernible in the figure.

Figure 13(b) employs color to illustrate variations in average pseudo-Hamiltonian energy across the two-parameter sets, reflecting systemic energy states. Consistent with Fig. 13(a), the system exhibits higher average energy in stable states and lower energy in chaotic regions. During periodic states, energy is distributed in an ordered manner within phase space, concentrated in a limited number of modes, resulting in higher average energy. In contrast, the energy of chaotic states is dispersed across multiple unstable orbits, leading to increased energy dissipation and lower average energy. This behavior aligns with experimental observations that biological neurons achieve higher energy efficiency during rhythmic firing activities. Comparison confirms the consistency between firing mode distribution and average energy: within suitable amplitude and temperature ranges, the system exhibits chaotic firing with relatively low average energy consumption, analogous to biological systems (e.g., homeotherms) operating within an optimal temperature range.

Comparing Figs. 13(a) and 13(b) further demonstrates that the distributions of firing mode and average pseudo-Hamiltonian energy are closely aligned. Within appropriate amplitude and temperature ranges, the system manifests chaotic firing with relatively low energy consumption, mirroring the operational patterns of biological systems, particularly homeothermic animals, under suitable environmental conditions.

4. Adaptive control

Thermoregulation in biological systems relies on the dynamic equilibrium of energy metabolism, encompassing positive and negative feedback loops as well as multiple regulatory mechanisms. This section introduces an adaptive control function in which temperature depends on pseudo-Hamiltonian energy, clarifying temperature-dependent neuronal firing mechanisms. Benchmark parameters are $\omega = 0.4\pi$, $a = 0.05$, $b = 0.05$, $c = 1.5$, $\eta = 0.2$, $l = 0.2$, $u_0 = 5$, $r_0 = 0.8$, $\sigma_1 = 0.01$, $H_0 = 0.5$, $\sigma_2 = 0.1$, $T_0 = 1.0$, $T_\mathrm{m} = 5.0$, with initial values $(0.2, 0.1, 0.02, 0.01)$.

This section examines mode transitions and pseudo-Hamiltonian energy changes during temperature-adaptive growth until saturation. The gain factor, attenuation factor, and energy threshold determine the temporal dynamics (e.g., time to saturation): increasing the gain factor or decreasing the energy threshold accelerates saturation (Figs. 14 and 15). The energy threshold represents the critical point for initiating metabolic responses. A lower energy threshold promotes metabolic heat production, thereby accelerating heat accumulation and system saturation.

Most biological systems, particularly homeotherms, have an upper temperature limit T_m, beyond which temperature no longer rises. Accordingly, the decay factor σ_2 and temperature ceiling jointly modulate the saturation magnitude and time: a smaller decay factor weakens heat dissipation, allowing metabolic heat production to remain unbalanced, thereby preventing stable saturation (Fig. 16). As metabolic heat drives temperature toward T_m, heat dissipation mechanisms become active; thus, T_m significantly influences both saturation magnitude and temporal dynamics (Fig. 17).

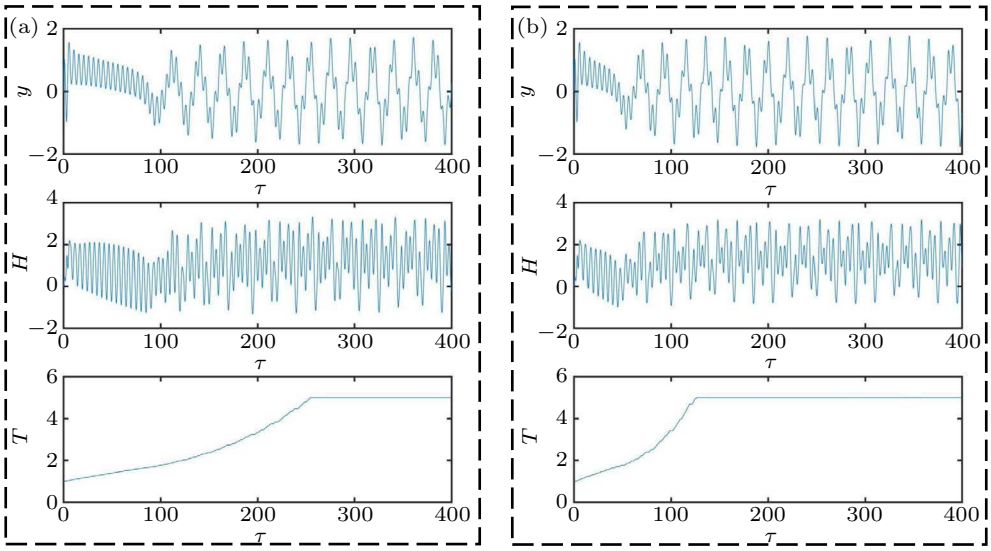


Fig. 14. Evolution of variable y, pseudo-Hamiltonian energy H, and temperature T under different gain coefficients: (a) $\sigma_1 = 0.01$; (b) $\sigma_1 = 0.02$.

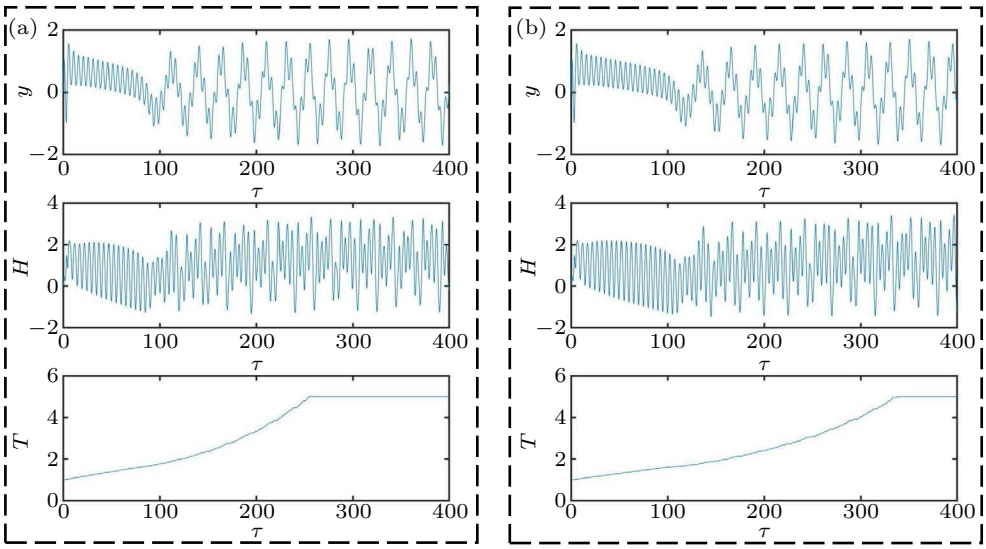


Fig. 15. Evolution of variable y, pseudo-Hamiltonian energy H, and temperature T under different energy thresholds: (a) $H_0 = 0.5$; (b) $H_0 = 1.0$.

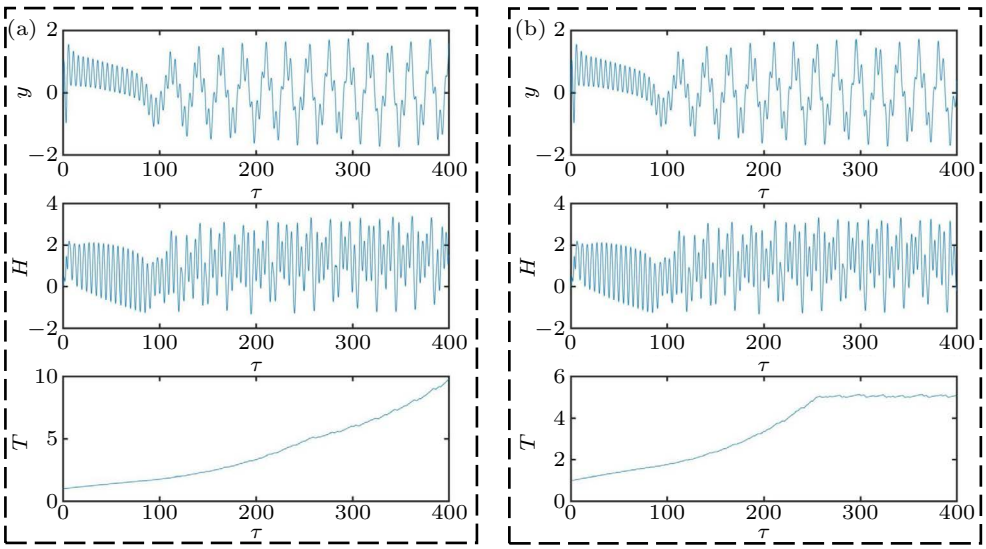


Fig. 16. Evolution of variable y, pseudo-Hamiltonian energy H, and temperature T under different attenuation factors: (a) $\sigma_2 = 0.02$; (b) $\sigma_2 = 0.04$.

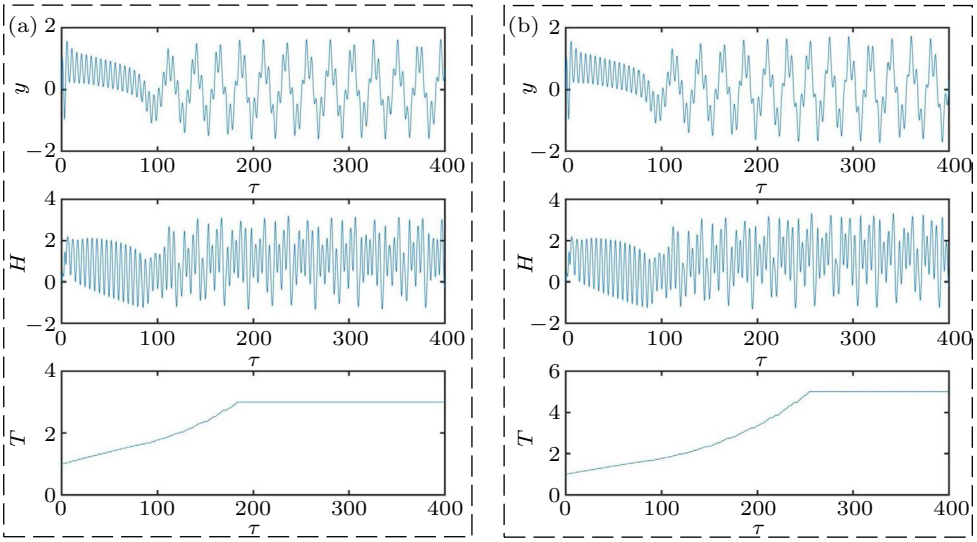


Fig. 17. Evolution of variable y, pseudo-Hamiltonian energy H, and temperature T under different ceiling temperatures: (a) $T_{\mathrm{m}} = 3.0$; (b) $T_{\mathrm{m}} = 5.0$.

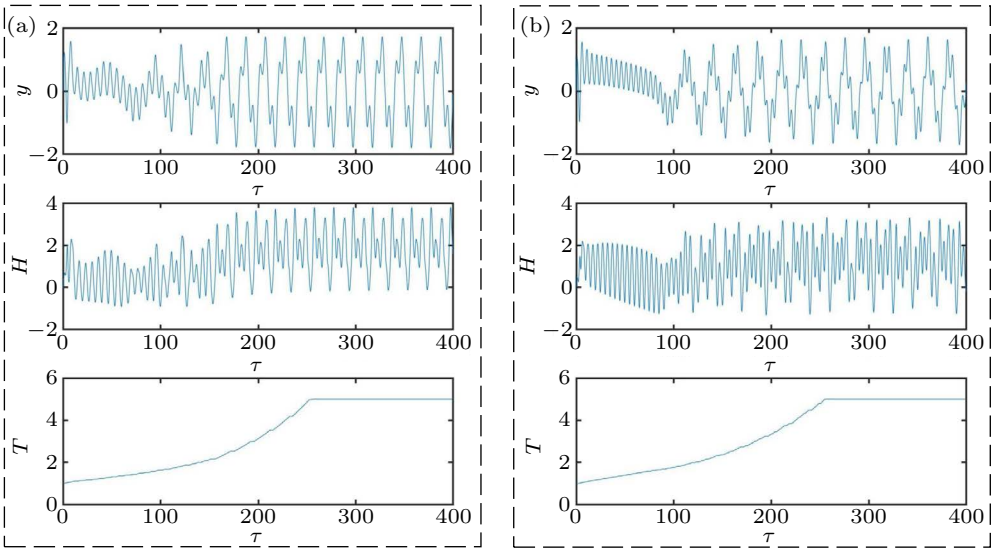


Fig. 18. Evolution of variable y, pseudo-Hamiltonian energy H, and temperature T under different phototube voltage frequencies: (a) $\omega = 0.3\pi$; (b) $\omega = 0.4\pi$.

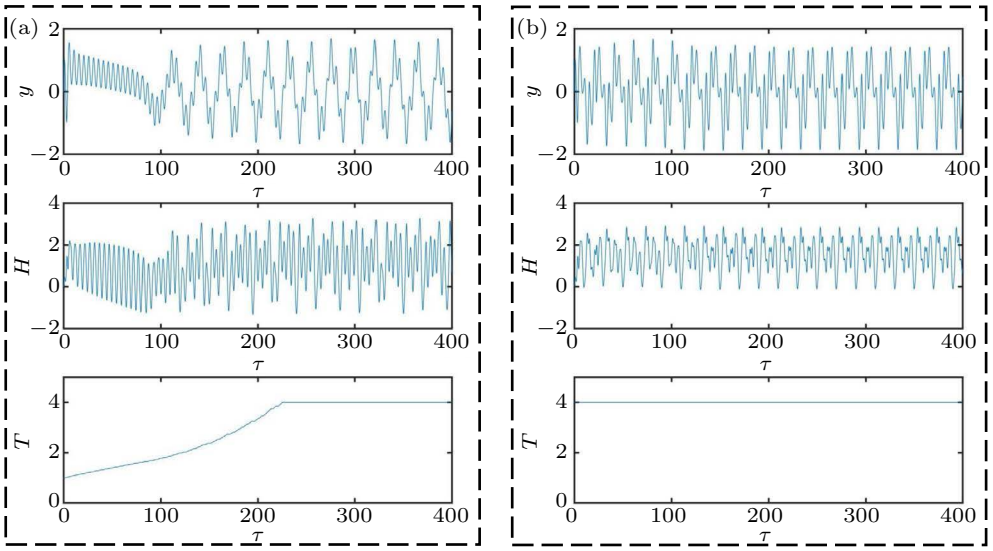


Fig. 19. Evolution of variable y, pseudo-Hamiltonian energy H, and temperature T at different initial temperatures. The ceiling temperature is $T_{\mathrm{m}} = 4.0$. (a) $T_0 = 1.0$; (b) $T_0 = 4.0$.

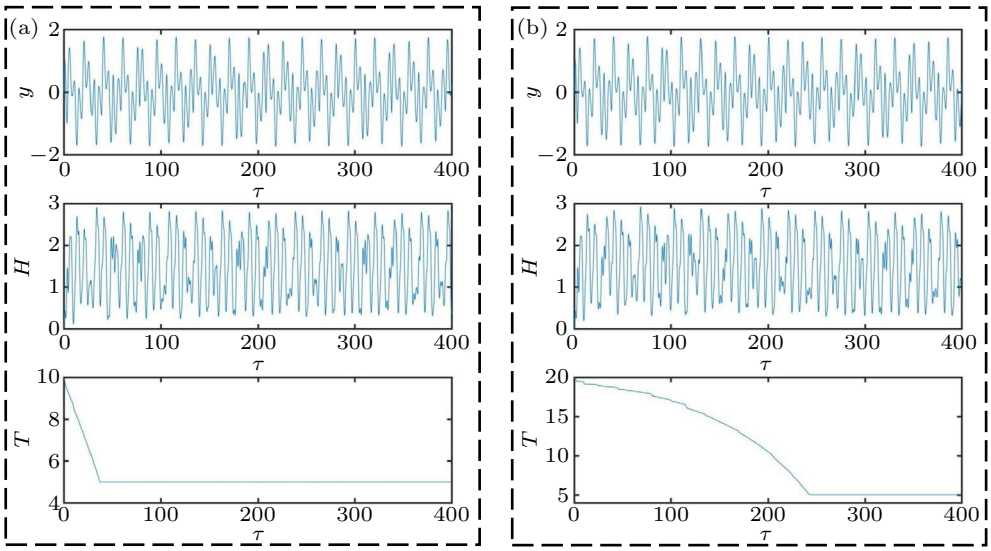


Fig. 20. Evolution of variable y, pseudo-Hamiltonian energy H, and temperature T at different initial temperatures. The attenuation factor is $\sigma_2 = 0.20$. (a) $T_0 = 10$; (b) $T_0 = 20$.

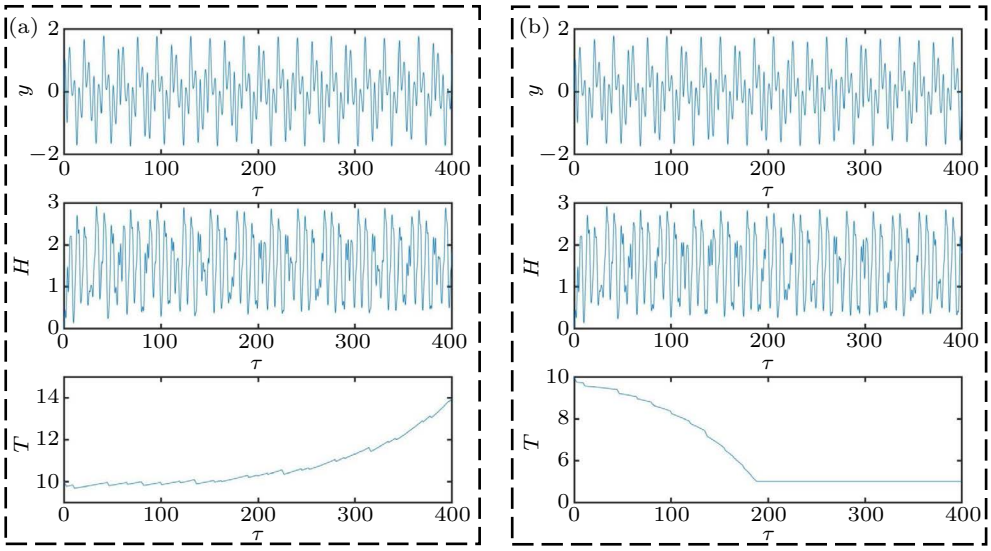


Fig. 21. Evolution of variable y, pseudo-Hamiltonian energy H, and temperature T at different attenuation factors. The initial temperature is $T_0 = 10$. (a) $\sigma_2 = 0.09$; (b) $\sigma_2 = 0.10$.

Neuronal firing patterns also impact temperature-adaptive control: varying external stimulus frequencies induce distinct oscillatory characteristics and affect temperature progression (Fig. 18).

The initial temperature T_0 strongly affects the system's variables (e.g., y), pseudo-Hamiltonian energy (H), and subsequent temperature evolution. Different initial temperature values generate distinct starting states and dynamic trajectories: when $T_0 < T_\mathrm{m}$, variable y and pseudo-Hamiltonian energy exhibit pronounced initial changes, followed by gradual temperature increase and stabilization; when $T_0 = T_\mathrm{m}$, no significant adjustments occur, and the final firing sequence differs (Fig. 19). Hence, varying initial temperatures produce different energy accumulation processes, leading to distinct neuronal firing evolution.

Beyond heating-phase adaptation, this study also investigates cooling-phase temperature adaptation (Figs. 20 and 21). Differences in initial states, such as metabolic rates or ion channel opening probabilities, modify the dynamic equilibrium between heat generation and dissipation. As a result, for identical attenuation factor σ_2, varying initial temperatures induce different cooling rates (Fig. 20). Conversely, for identical initial temperatures, the attenuation factor σ_2 substantially affects temperature evolution (Fig. 21): a larger σ_2 enhances heat dissipation, whereas values below a critical threshold cause dissipation to lag behind generation, resulting in gradual temperature increase through heat accumulation.

5. Conclusion

This study presents a biomimetic neuron circuit capable of multimodal photothermal perception. By integrating a memristor-connected dual-capacitor structure with a photo-

tube and thermistor, the circuit effectively emulates the biophysical properties of neuronal membranes and their responsiveness to both light and temperature stimuli.

Parameter-dependent firing patterns Variations in capacitance ratio, phototube voltage amplitude and frequency, temperature, and thermistor reference resistance induce transitions between periodic and chaotic firing. Periodic states are associated with higher average pseudo-Hamiltonian energy, whereas chaotic states occur within specific parameter ranges.

Dual-parameter interactions Phototube voltage amplitude and temperature synergistically influence firing modes, with chaotic behavior confined to distinct parameter regions. Lower temperatures tend to stabilize quasi-quiescent states, while appropriately higher temperatures expand the range of stimulus intensities capable of eliciting chaotic firing.

Adaptive temperature regulation The system's temperature dynamics, governed by pseudo-Hamiltonian energy, are modulated by gain and attenuation factors, energy thresholds, and temperature ceilings. Both heating and cooling phases exhibit adaptive behavior, with initial temperature and dissipation capacity (attenuation factor) determining thermal equilibrium rates and saturation characteristics.

This model provides a theoretical framework for investigating neuronal energy metabolism and photothermal sensory integration, offering insights into biological neural encoding mechanisms. Future work will focus on hardware validation using FPGA or analog circuits and extending the model to applications in biomimetic sensors, neuromorphic computing, and intelligent systems, highlighting its potential for advancing artificial perception technologies.

It should be noted that the current model does not yet account for environmental variability. Subsequent studies will incorporate stochastic perturbations to explore phenomena such as stochastic resonance, and will further investigate multi-sensory integration and learning mechanisms, aiming to enhance the model's generality and functional versatility.

Acknowledgment

This work was supported by the Natural Science Foundation of Chongqing (Grant No. CSTB2024NSCQ-MSX0944).

References

[1] Gundersen V, Storm-Mathisen J and Bergersen L H 2015 *Physiol. Rev.* **95** 695
[2] Harris K D and Mrsic-Flogel T D 2013 *Nature* **503** 51
[3] Walker E Y, Sinz F H, Cobos E, Muhammad T, Froudarakis E, Fahey P G, Ecker A S, Reimer J, Pitkow X and Tolias A S 2019 *Nat. Neurosci.* **22** 2060
[4] Wang Y Q, Hartung J E, Goad A, *et al.* 2024 *Adv. Healthc. Mater.* **13** 2302330
[5] Gracheva E O, Ingolia N T, Kelly Y M, Cordero-Morales J F, Hollopeter G, Chesler A T, Sáchez E E, Perez J C, Weissman J S and Julius D 2010 *Nature* **464** 1006
[6] Zhang K X, D'Souza S, Upton B A, *et al.* 2020 *Nature* **585** 420
[7] Guo, X E, Sun, Z D, Zhu, Y, *et al.* 2024 *Adv. Mater.* **36** 2406778
[8] Sharma K and Sharma M 2023 *Environ. Res.* **236** 116826
[9] Blasch E, Cruise R, Aved A J, Majumder U K and Rovito T V 2019 *AI Mag.* **40** 50
[10] Wang Y, Garg R, Cohen-Karni D and Cohen-Karni T 2023 *Nat. Rev. Bioeng.* **1** 193
[11] Richter L M A and Gjorgjieva J 2017 *Curr. Opin. Neurobiol.* **46** 39
[12] Mishra A, Ghosh S, Dana S K, Kapitaniak T and Hens C 2021 *Chaos* **31** 052101
[13] Xie Y, Yao Z, Hu X and Ma J 2022 *Chin. Phys. B* **30** 120510
[14] Zhou P, Zhang X, Hu X and Ren G 2022 *Nonlinear Dynam.* **110** 1879
[15] Hu X, Zhu S, Yang J, Yao Z, Zhou P and Ma J 2024 *Commun. Theor. Phys.* **76** 105004
[16] Apata C O, Tang Y R, Zhou Y F, Jiang L and Pei Q M 2024 *Chin. Phys. B* **33** 58704
[17] Bloom M, Evans E and Mouritsen O G 1991 *Q. Rev. Biophys.* **24** 293
[18] Guo Q, Zhou P, Zhang X and Zhu Z 2025 *Cogn. Neurodynamics* **19** 75
[19] Chai X, Wang X, Zhang J, Kong D and Sun G 2025 *Commun. Theor. Phys.* **77** 105003
[20] Yang F F, Ma J and Ren G D 2024 *J. Theor. Biol.* **578** 111686
[21] Wan J Y, Wu F Q, Ma J and Wang W 2024 *Chin. Phys. B* **33** 050504
[22] Yang X, Taylor B, Wu A, Chen Y and Chua L O 2022 *IEEE T. Circuits-I* **69** 1845
[23] Yang F F, Ma J and Wu F Q 2024 *Chaos Soliton. Fract.* **187** 115361
[24] Jiang W, Li J, Liu H, Qian X, Ge Y, Wang L and Duan S2022 *Chin. Phys. B* **31** 040702
[25] Shang C, Sun K, Wang H, Yao Z and He S 2023 *Nonlinear Dynam.* **111** 20347
[26] Xu L, Qi G Y and Ma J 2022 *Appl. Math. Model.* **101** 503
[27] Ding Q, Wu Y, Li T, Yu D and Jia Y 2023 *Chaos Soliton. Fract.* **171** 113464
[28] Njitacke Z T, Awrejcewicz J, Ramakrishnan B, Rajagopal K and Kengne J 2022 *Nonlinear Dynam.* **107** 2867
[29] Li Y N, Ma J and Xie Y 2024 *Nonlinear Dynam.* **112** 7459
[30] Xu Y, Liu M, Zhu Z and Ma J 2020 *Chin. Phys. B* **29** 098704
[31] Yeh F, Jara-Oseguera A and Aldrich R W 2023 *P. Natl. Acad. Sci. USA* **120** e2301528120
[32] Fossi J T, Deli V, Edima H C, Njitacke Z T, Feudjio K F and Atangana J 2022 *Eur. Phys. J. B* **95** 66
[33] Hu X K, Yang J, Song Z and Zhou P 2025 *Phys. Scripta* **100** 075232
[34] Jia J, Zhou P, Zhang X and Ma J 2024 *AEU-Int. J. Electron. C.* **174** 155069
[35] Sarasola C, Torrealdea F J, d'Anjou A, Moujahid A and Graña M 2004 *Phys. Rev. E* **69** 011606
[36] Alonso L M and Marder E 2020 *eLife* **9** e55470
[37] Wendering P and Nikoloski Z 2023 *Biotechnol. Adv.* **67** 108203
[38] Wu F Q, Guo Y T and Ma J 2023 *Sci. China Technol. Sc.* **66** 3139